# Single-photon excitation of a coherent state: Catching the elementary step of stimulated light emission

Alessandro Zavatta, Silvia Viciani, and Marco Bellini*
*Istituto Nazionale di Ottica Applicata, L.go E. Fermi, 6, I-50125, Florence, Italy*
*and LENS and Department of Physics, University of Florence, I-50019 Sesto Fiorentino, Florence, Italy*
(Received 11 March 2005; revised manuscript received 20 June 2005; published 23 August 2005)

When a single quantum of electromagnetic field excitation is added to the same spatiotemporal mode of a coherent state, a new field state is generated that exhibits intermediate properties between those of the two parents. Such a single-photon-added coherent state is obtained by the action of the photon creation operator on a coherent state and can thus be regarded as the result of the most elementary excitation process of a classical light field. Here we present and describe in depth the experimental realization of such states and their complete analysis by means of a novel ultrafast, time-domain, quantum homodyne tomography technique clearly revealing their nonclassical character.

DOI: 10.1103/PhysRevA.72.023820 PACS number(s): 42.50.Dv, 03.65.Wj

## I. INTRODUCTION

A coherent state $|\alpha\rangle$, the eigenstate of the photon annihilation operator $\hat{a}|\alpha\rangle=\alpha|\alpha\rangle$, is the closest analog to a classical light field and exhibits a Poisson photon number distribution with an average photon number of $|\alpha|^2$ and a width of $|\alpha|$. Coherent states possess well defined amplitude and phase, whose uncertainties are the minimum permitted by the Heisenberg uncertainty principle. On the contrary, a Fock state, the eigenstate of the photon number operator $\hat{a}^\dagger\hat{a}|n\rangle=n|n\rangle$, contains a perfectly defined number of quanta of field excitation and is strictly quantum mechanical, with no classical analog. Moreover, being the intensity of a Fock state defined without uncertainty, its phase is completely undefined.

Single-photon Fock states have been recently generated by means of conditional preparation techniques and homodyne tomography has been used to completely characterize them with the reconstruction of an associated Wigner function clearly exhibiting negative values [1,2]. Displaced Fock states, obtained by mixing a coherent state with a single photon upon a highly reflecting beam splitter as in Ref. [3], have also been investigated with tomographic techniques which have shown the non-Gaussian character of their marginal distributions and negative values of the Wigner function. Other nonclassical states have recently been produced starting from a squeezed vacuum and with the controlled subtraction of a single photon: in this case the marginal distributions clearly showed a squeezed and non-Gaussian character but the preparation and detection efficiency was not high enough to reconstruct a negative-valued Wigner function [4].

We have recently reported [5] the experimental generation of a new kind of nonclassical field states and their tomographic analysis based on time-resolved homodyne detection, which has allowed us to observe both the squeezed character and the negativity of the associated Wigner function. These so-called single-photon-added coherent states are produced whenever a single photon is injected in the same spatiotemporal mode of a coherent state and are shown to exhibit a mix of the characteristics of both parents. In particular, by simply varying the contribution of the initial coherent state, the character of the final state can be continuously tuned between completely quantum and almost completely classical.

Here we report an in-depth tomographic analysis of such states based on new and more accurate experimental data and comprising a complete comparison of the reconstructed density matrix elements with those expected from a fully developed theory. This has allowed us to follow in a much more detailed way the evolution of the generated state from the particlelike one, characterized by a circularly symmetric and negative-valued single-photon Wigner function, through a squeezed intermediate region characterized by the gradual appearance of a phase, towards the wavelike classical coherent state.

In addition to the interesting physical properties of single-photon-added coherent states, the ability to generate, manipulate and characterize such states can be useful for possible future applications in the engineering of quantum states [6,7] and in quantum information protocols [4].

## II. PROPERTIES OF THE SPACS

In 1991, Agarwal and Tara [8] introduced a new class of states, defined by the repeated ($m$ times) application of the photon creation operator to the coherent state

$$|\alpha,m\rangle = k_{\alpha,m}\hat{a}^{\dagger m}|\alpha\rangle, \tag{1}$$

with $k_{\alpha,m}=[m!L_m(-|\alpha|^2)]^{-1/2}$ a normalization factor where $L_m(x)$ is the $m$th-order Laguerre polynomial and $m$ is an integer. Such photon-added coherent states (PACSs) essentially represent the result of successive elementary one-photon excitations of a classical coherent field and occupy an intermediate position between the Fock and the coherent states, reducing to the two limit cases for $\alpha\to 0$ or $m\to 0$, respectively. From the expansion of PACSs in terms of Fock

*Electronic address: bellini@inoa.it

 

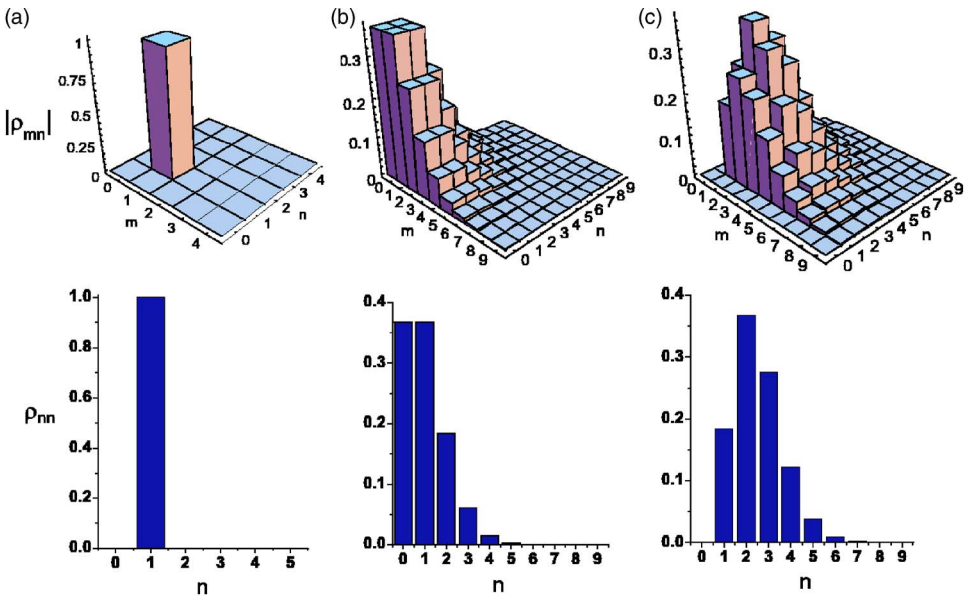


FIG. 1. (Color online) Theoretical density matrix elements and photon number distributions for (a) the single-photon Fock state $|1\rangle$, (b) the coherent state $|\alpha\rangle$ (with $|\alpha|=1$), and (c) the corresponding SPACS $|\alpha,1\rangle$ obtained by emission of a single photon in the mode of the coherent state.

states, it can be easily seen that they essentially correspond to a shifted version of a coherent state where all the $|n\rangle$ terms with $n<m$ are missing and that all the elements of the corresponding density matrix are re-scaled and displaced towards higher indices $\rho_{i,j}\rightarrow\rho_{i+m,j+m}$, leaving all the elements with $i,j<m$ void.

When just a single quantum of field excitation is added to a coherent field, the single-photon-added coherent state (SPACS) reads

$$|\alpha,1\rangle=\frac{\hat{a}^{\dagger}|\alpha\rangle}{\sqrt{1+|\alpha|^2}} \tag{2}$$

and can be also viewed as the superposition of a displaced single-photon Fock state and a coherent state [8]. SPACSs can be expanded in terms of Fock states as

$$|\alpha,1\rangle=\frac{e^{-|\alpha|^2/2}}{\sqrt{1+|\alpha|^2}}\sum_{n=0}^{\infty}\frac{\alpha^n}{\sqrt{n!}}\sqrt{n+1}|n+1\rangle, \tag{3}$$

where the lack of the vacuum term contribution is evident. Accordingly, the density matrix elements for the SPACSs are

$$\rho_{i,j}^{|\alpha,1\rangle}=\frac{ij}{\sqrt{i\,!\,j!}}\frac{e^{-|\alpha|^2}}{1+|\alpha|^2}\alpha^{(i-1)}\alpha^{*(j-1)} \tag{4}$$

and the effect of single-photon excitation can be readily observed in the plots of Figs. 1, where the absolute value of the theoretical matrix elements and the photon number distributions (their diagonal elements) are reported for the single-photon Fock state, for a coherent state with $|\alpha|=1$ and for the corresponding SPACS.

Unlike the operation of photon annihilation, which maps a coherent state into another coherent state ($\hat{a}|\alpha\rangle=\alpha|\alpha\rangle$), i.e., a classical field into another classical field, the single-photon excitation of a coherent state changes it into something quite different, especially for low values of $\alpha$, where the absence of the vacuum term has a stronger impact. In the extreme case of an initial vacuum state $|0\rangle$, the addition of one photon indeed transforms it into the very nonclassical single-photon Fock state $|1\rangle$, which exhibits negative values of the Wigner function around the origin (see Fig. 2). More generally, the Wigner function for a single-photon-added coherent state of arbitrary amplitude $\alpha$ can be expressed as

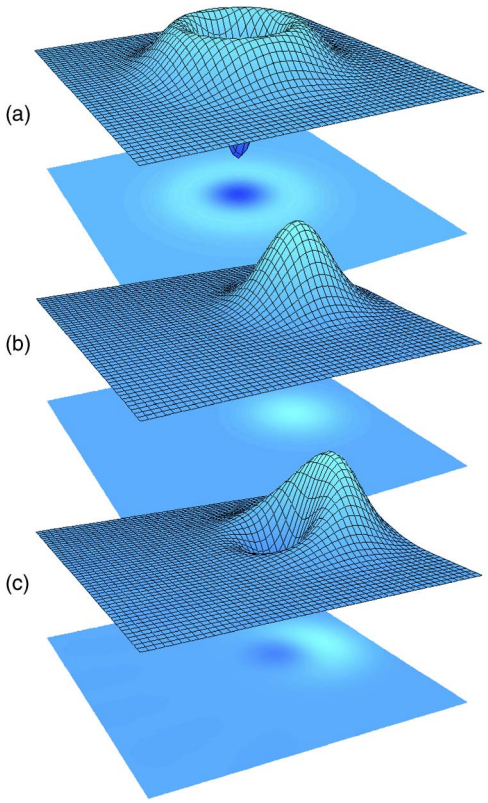


FIG. 2. (Color online) Theoretical Wigner function for (a) the single-photon Fock state $|1\rangle$, (b) the coherent state $|\alpha\rangle$, (c) the SPACS $|\alpha,1\rangle$. A value of $|\alpha|=1$ is used.

$$W(z) = \frac{-2(1-|2z-\alpha|^2)}{\pi(1+|\alpha|^2)} e^{-2|z-\alpha|^2} \tag{5}$$

(where $z=x+iy$) and can clearly become negative, a proof of its nonclassical character, whenever the condition

$$|2z-\alpha|^2 < 1 \tag{6}$$

is satisfied. Thus, in general, the application of the creation operator $\hat{a}^\dagger$, changes a completely classical coherent state into a quantum state with a varying degree of nonclassicality, which becomes more evident the smaller the initial amplitude of the $|\alpha\rangle$ state. If the amplitude $\alpha$ is gradually increased from zero, the smooth transition from an initial purely quantum state (the single-photon Fock state) towards a classical coherent one (with the birth and the gradual appearance of a well defined phase) can be achieved.

In addition to the negativity of the Wigner function, SPACSs also exhibit a definite squeezing in their field quadratures that can be readily observed. Given a field quadrature $\hat{x}_\theta = \frac{1}{2}(\hat{a}e^{-i\theta} + \hat{a}^\dagger e^{i\theta})$, its mean value is

$$\langle x_\theta \rangle_\alpha = \langle \alpha, 1|\hat{x}_\theta|\alpha, 1\rangle = \frac{|\alpha|(2+|\alpha|^2)\cos(\theta)}{1+|\alpha|^2} \tag{7}$$

and its fluctuations amount to

$$[\Delta x_\theta]^2_\alpha = \langle x^2_\theta \rangle_\alpha - \langle x_\theta \rangle^2_\alpha = \frac{1}{4} + \frac{1-|\alpha|^2\cos(2\theta)}{2(1+|\alpha|^2)^2}. \tag{8}$$

Clearly, the quadrature obtained by choosing $\theta=0$ exhibits reduced fluctuations with respect to the coherent state for $|\alpha|>1$, and is thus squeezed. It is interesting to note that, differently from Fock and Gaussian squeezed states, SPACSs combine both the key features normally associated to quantum states: the negativity of the Wigner function and the reduced fluctuations along one quadrature.

## III. GENERATION OF THE SPACS

SPACSs can be generated by injecting a coherent state $|\alpha\rangle$ into the signal mode of an optical parametric amplifier and exploiting the stimulated emission of a single down-converted photon into the same mode. Differently from conventional optical amplification where a coherent state is converted to another coherent state, here a low-gain regime of the amplifier and a conditioning of the state based on measurements on the idler mode are required to exactly select the one-photon excitation term (i.e., to avoid higher-order excitations which cannot be discriminated by our single-photon detectors and to exclude the vacuum contribution). Hence, in order to make sure that single-photon emission has taken place in the signal channel, one can use a conditional preparation technique which guarantees the generation of the target state every time that a single photon is detected in the correlated idler mode.

The Hamiltonian for the parametric amplifier reads

$$\hat{H} = i\hbar\chi(\hat{a}^\dagger_s\hat{a}^\dagger_i - \hat{a}_s\hat{a}_i), \tag{9}$$

where $\hat{a}_i$ ($\hat{a}_s$) is the annihilation operator for the idler (signal) mode and $\chi$ is proportional to the amplitude of the (classical) pump and to the second-order susceptibility of the medium. The time evolution of an initial state $|\psi(0)\rangle$ is thus described by

$$|\psi(t)\rangle = e^{-i(\hat{H}t/\hbar)}|\psi(0)\rangle = e^{\chi t(\hat{a}^\dagger_s\hat{a}^\dagger_i - \hat{a}_s\hat{a}_i)}|\psi(0)\rangle. \tag{10}$$

If the parametric gain is kept sufficiently low ($g=\chi t \ll 1$), which is always the case in our experimental situation, the final output state can be approximated as

$$|\psi(t)\rangle = [1 + g(\hat{a}^\dagger_s\hat{a}^\dagger_i - \hat{a}_s\hat{a}_i)]|\psi(0)\rangle. \tag{11}$$

By letting a seed coherent field $|\alpha\rangle_s$ enter the parametric crystal in the signal mode, while vacuum ($|0\rangle_i$) enters in the idler channel, the final state becomes

$$|\psi\rangle = [1 + g(\hat{a}^\dagger_s\hat{a}^\dagger_i - \hat{a}_s\hat{a}_i)]|\alpha\rangle_s|0\rangle_i = |\alpha\rangle_s|0\rangle_i + g\hat{a}^\dagger_s|\alpha\rangle_s|1\rangle_i \tag{12}$$

and the output signal mode will mostly contain the original coherent state, except for the few cases when the state $|1\rangle_i$ is detected in the idler output mode. These relatively rare detection events, which take place with a probability proportional to $|g|^2(1+|\alpha|^2)$, project the signal state onto the desired SPACS $|\alpha,1\rangle_s$, corresponding to the stimulated emission of one photon in the same mode of $|\alpha\rangle$. Note that when the input state is of the form $|0\rangle_s|0\rangle_i$, i.e., no seed coherent field is injected into the crystal, spontaneous parametric down conversion takes place starting from the input vacuum fields and pairs of entangled signal and idler photons with random (but mutually correlated) phases are produced in the crystal in the state $|1\rangle_s|1\rangle_i$ with a low probability proportional to $|g|^2$. In this case, the detection of a single photon in the idler mode projects the signal state onto a single-photon Fock state and, by following the evolution of the final quantum state while the amplitude $\alpha$ increases from zero, one can witness the gradual transition from the spontaneous to the stimulated regimes of light emission with the smooth transformation of a single photon (particlelike) state towards a coherent (wavelike) one.

Quite interestingly, one can obtain an absolute calibration of the amplitude of the seed coherent field $|\alpha\rangle_s$ injected in the SPDC signal mode by measuring the rate of counts in the idler channel and comparing them to the unseeded case. As stated above, the ratio of such rates equals $(1+|\alpha|^2)$ and this is clearly due to the enhancement of emission probability characteristic of stimulated emission in bosonic fields. The same scheme was originally proposed by Klyshko [9] as a metrological tool for absolute radiance measurements [10,11].

For low $\alpha$ values, one can truncate the above expressions to the first two terms of the coherent state expansion in the number state basis. In this case the final state becomes

$$\begin{aligned}|\psi\rangle &\approx [1 + g(\hat{a}^\dagger_s\hat{a}^\dagger_i - \hat{a}_s\hat{a}_i)](|0\rangle_s + \alpha|1\rangle_s)|0\rangle_i \\ &= (|0\rangle_s + \alpha|1\rangle_s)|0\rangle_i + g(|1\rangle_s + \sqrt{2}\alpha|2\rangle_s)|1\rangle_i\end{aligned} \tag{13}$$

and the conditioning thus reduces the signal state to the coherent superposition $|1\rangle_s + \sqrt{2}\alpha|2\rangle_s$. Note that such a coherent superposition of two number states possesses a well defined

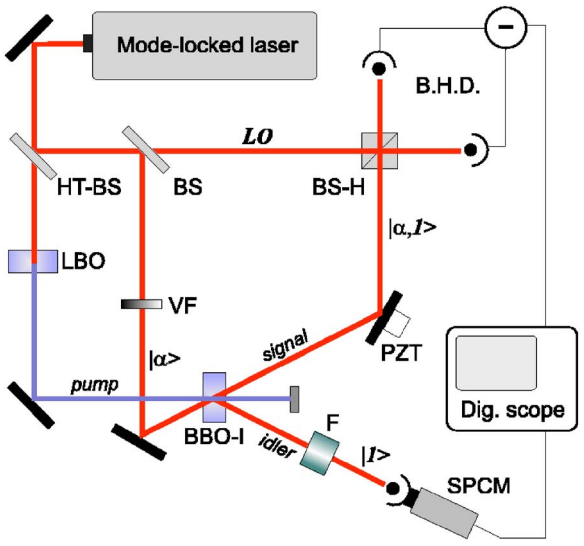


FIG. 3. (Color online) Experimental apparatus. HT-BS: high transmission beam splitter, LBO: lithium triborate crystal, BS and BS-H: 50% beam-splitters, VF: variable attenuation filter, BBO-I: type-I $\beta$-barium borate down-converter crystal, PZT: piezoelectric transducer, BHD: balanced homodyne detector, F: spectral and spatial filters, SPCM: single photon counting module, LO: local oscillator.

phase and is highly nonclassical, completely missing the contribution of the vacuum.

The same state as the one described by Eqs. (12) and (13) has been recently generated and used by Resch *et al.* [12] to generate an arbitrary superposition of zero- and one-photon states. In that case, however, the conditioning was performed upon the detection of a single photon in the same mode $|1\rangle_s$ of the input coherent state, hence the final state was completely different from the ones investigated here, and of the form $(\alpha|0\rangle_i+g|1\rangle_i)$. The injection of a single photon instead of a coherent state as a seed for conditional parametric amplification has also been investigated in Ref. [13] and experimentally demonstrated [14], with the amplification to a $|2\rangle_s$ Fock state in the context of quantum cloning.

## IV. EXPERIMENTAL SETUP

The experimental apparatus used to generate and analyze the SPACS is schematically drawn in Fig. 3. A mode-locked Ti:sapphire laser, emitting 1–2-ps-long pulses at 786 nm and at a repetition rate of 82 MHz is used as the primary source. The laser pulses are frequency doubled to 393 nm in a 13-mm-long LBO crystal which thus produces the pump pulses for parametric down conversion in a 3-mm-thick type-I BBO crystal. The crystal is slightly tilted from the collinear configuration in order to obtain an exit cone beam with an angle of $\sim 3°$ from which symmetric signal and idler modes are roughly selected by means of irises placed at about 70 cm from the crystal.

In order to nonlocally select a pure state on the signal channel, idler photons undergo narrow spatial and frequency filtering before detection; indeed the nonlocally prepared signal state will only approach a pure state if the filter transmission function is much narrower than the momentum and spectral widths of the pump beam generating the SPDC pair [15–18]. The idler beam is thus passed through a pair of etalon interference filters which perform a narrow (50 GHz) spectral selection and is then coupled into a single-spatial-mode fiber before impinging onto a single photon counting module (Perkin-Elmer SPCM AQR-14).

The weak coherent state $\alpha$ is obtained by controlled attenuation (VF in the figure, composed of a polarizer and a half-wave plate) of a small portion of the laser emission which is fed into the signal mode of the parametric crystal and is then directed to a 50% beam splitter (BS-H in figure). Here it is overlapped with a second (intense) coherent state (again obtained from a portion of the original laser pulses) which is spatially mode matched to the conditionally prepared SPACS by the insertion of appropriate lens combinations (not shown in the figure) along its path and serves as the local oscillator (LO) for the homodyne measurements [19]. In order to finely adjust the alignment and the synchronization between the signal and LO pulses, we use the stimulated beam produced by injecting a different seed pulse into the idler channel of the parametric crystal. Under appropriate conditions [16], the beam generated by stimulated emission on the signal channel is emitted in a spatial mode which closely matches that of the target signal beam and can thus be used for alignment purposes. Measurements are performed at different values of the coherent seed amplitude $|\alpha|$ by rotating the half-wave plate; as seen above, a calibration of such an amplitude is simply obtained from a measurement of the increase in the idler count rate.

## V. TIME-DOMAIN HOMODYNE MEASUREMENTS

The pulsed homodyne detection scheme used to analyze the quantum states has been recently developed by our group and is currently the only system capable of operating at the full repetition rate (80 MHz) of common mode-locked lasers in the time domain [2,20]. The fields at the two output ports of the beam splitter are detected by two photodiodes (Hamamatsu S3883, with active area 1.7 $mm^2$) whose difference signal is amplified and sent to a fast digital oscilloscope whose acquisition is triggered by the detection events in the idler channel. Each acquisition frame spans two consecutive LO pulses where only the first one is synchronized with the detection of an idler photon and contains the "information" about the SPACS $|\alpha,1\rangle_s$, while the second one can be used for the measurement of the reference unexcited coherent state $|\alpha\rangle_s$. By blocking the seed coherent pulse, the single-photon Fock state $|1\rangle_s$ and the LO shot-noise distributions corresponding to the vacuum state $|0\rangle_s$ are simultaneously measured. About 5000 acquisition frames can be stored sequentially in the scope at a maximum rate of 160 000 frames per second. Each sequence of frames is then transferred to a personal computer where the areas of the pulses are measured and their statistic distributions are analyzed in real time.

If a narrow temporal gate with the laser pulses is used, the typical rate of state preparation for vacuum input is about

$300\ s^{-1}$, with less than 1% contribution from accidental counts. A typical sequence of about 5000 acquisition frames can thus be captured and analyzed in about 20–30 s when no coherent seed is fed in the signal mode. It is interesting to remind the reader that the probability of detecting an idler photon is proportional to $|\hat{a}^{\dagger}|\alpha\rangle|^2$, hence, as soon as $\alpha$ is increased and stimulated emission starts taking place, the rate of trigger events grows proportional to $(1+|\alpha|^2)$, thus making the acquisition rate much higher. However, even at the maximum values ($|\alpha|\approx 7$) reached in the experiments, the trigger rate never exceeds $2\times 10^4\ s^{-1}$ (to be compared with the laser pulse repetition rate of about $8\times 10^7\ s^{-1}$), so that the probability of conditioning the measurement upon more than a single idler photon always remains negligible.

To explore the different quadratures of the generated field, its phase $\theta$ relative to the LO field has been varied in controlled steps by applying a voltage to a piezoelectric transducer (PZT) which slightly translates one of the steering SPACS mirrors. A very good passive stabilization of the large (about 2-m long) Mach-Zehnder-like interferometer formed by the paths of the LO and of the seed coherent beam has been achieved in order to guarantee a constant relative phase during the acquisition of a frame sequence. This is extremely tricky especially for low values of $\alpha$, where the acquisition rate is lowest. About 50 acquisitions were performed at each value of the coherent seed amplitude $\alpha$ for 10–15 phase values in the $[0,\pi]$ interval.

In order to reduce the contribution from low-frequency noise in the detection system, the amplified difference signal from the two photodiodes is ac coupled (cutoff frequency of about 3 kHz at −3 dB) before subsequent amplification and acquisition. This high-pass filter, combined with the temporal sampling operated by the software for the measurement of the pulse areas, results in a reduced contribution from the dc terms in the acquired homodyne data which has to be taken into account in the analysis. While the fast pulse-to-pulse fluctuations which contribute to the marginal distributions are not affected by such filtering, the mean value of such distributions has to be scaled by a factor that depends on the sampling window used to measure the pulse area. This is clearly not an issue when measuring the vacuum field or Fock states, since the mean value of their marginal distributions is constantly zero, but it has to be carefully considered when dealing with states having a non-null mean field value. A calibration of such a factor can be simply carried out by comparing the sequence of marginal distributions as measured for the coherent state and the value of $\alpha$ as obtained from the idler counts, and can then be used to rescale all the mean marginal values before subsequent analysis. This procedure was also double checked by fitting the experimental SPACS marginals to the expected theoretical shapes and obtaining an independent measure of $|\alpha|$ to compare with the one deduced from the idler counts.

## VI. DATA ANALYSIS AND DISCUSSION

Balanced homodyne detection allows the measurement of the signal electric field quadratures $\hat{x}_\theta=\hat{x}\cos\theta+\hat{y}\sin\theta$ as a function of the relative phase $\theta$ imposed between the LO and the signal, where the two orthogonal field quadratures $\hat{x}$ and $\hat{y}$ are defined as $\hat{x}=\frac{1}{2}(\hat{a}+\hat{a}^{\dagger})$ and $\hat{y}=(i/2)(\hat{a}^{\dagger}-\hat{a})$ and $[\hat{x},\hat{y}]=i/2$. By performing a series of homodyne measurements on equally prepared states it is possible to obtain the probability distributions $p(x,\theta)$ of the quadrature operator $\hat{x}_\theta=\frac{1}{2}(\hat{a}e^{-i\theta}+\hat{a}^{\dagger}e^{i\theta})$ that are simply seen to correspond to the marginals of the Wigner quasiprobability distribution $W(x,y)$ [21]:

$$p(x,\theta)=\int_{-\infty}^{+\infty} W(x\cos\theta-y\sin\theta, x\sin\theta+y\cos\theta)dy. \tag{14}$$

Given a sufficient number of quadrature distributions at different values of the phase $\theta\in[0,\pi]$, one is able to reconstruct the quantum state of the field under study [22]. The elements of the density matrix $\hat{\rho}$ of the state in the number-state representation can be obtained by averaging the so called "pattern functions" $f_{nm}(x,\theta)$ over the outcomes of the quadrature operator and over the phase $\theta$ as

$$\langle n|\hat{\rho}|m\rangle=\frac{1}{\pi}\int_0^{\pi} d\theta\int_{-\infty}^{+\infty} dx\, p(x,\theta)f_{nm}(x,\theta), \tag{15}$$

where the pattern functions can be implemented for unit quantum efficiency with stable numerical algorithms [22,23]. The Wigner function can then be obtained by means of the following transformation:

$$W(x,y)=\sum_{n,m}^{M}\rho_{n,m}W_{n,m}(x,y), \tag{16}$$

where $W_{n,m}(x,y)$ is the Wigner function of the operator $|n\rangle\langle m|$. Note that, using this procedure, the Wigner function of the state is reconstructed from a truncated density matrix of dimension $M\times M$. This implies a finite resolution in the reconstructed function which, however, can be adapted to the particular physical situation of interest in order to avoid loss of information on the state. In Fig. 4 a sequence of SPACS

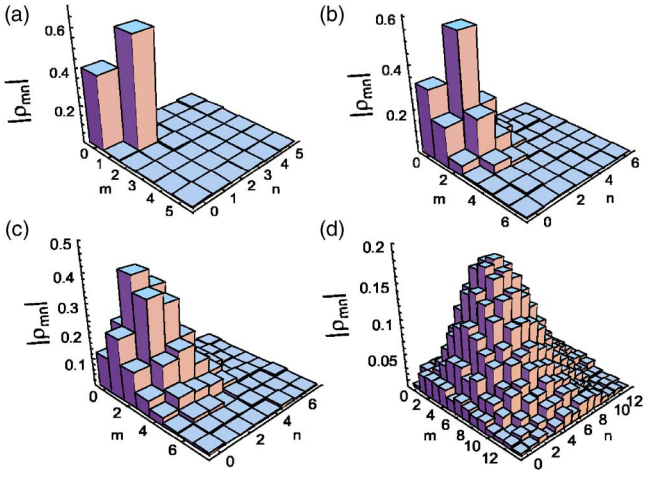


FIG. 4. (Color online) Density matrices of the SPACSs as reconstructed from the experimental data for increasing values of the seed amplitude. (a) $|\alpha|=0$, i.e., single photon Fock state, (b) $|\alpha|=0.387$, (c) $|\alpha|=0.955$, (d) $|\alpha|=2.61$.

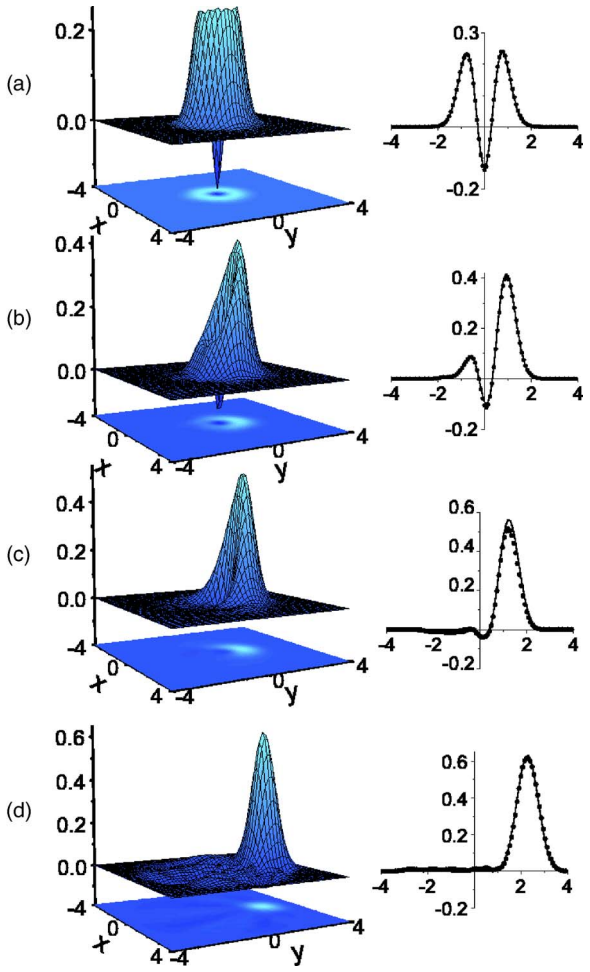


FIG. 5. (Color online) Wigner functions of the SPACSs as reconstructed from the density matrix elements shown in Fig 4. Also shown are sections of the reconstructed Wigner functions in the $x=0$ plane (data points), together with the ones (solid lines) calculated as explained below by taking the limited efficiency of the system into account.

reconstructed density matrices is shown for increasing values of the seed coherent field amplitudes $|\alpha|$.

In Fig. 5 the corresponding Wigner functions, obtained from the truncated density matrices of Fig 4 are shown: the first one (a), obtained with a blocked input, corresponds to the single-photon Fock state obtained by conditional preparation from the two-photon wave function of SPDC [1,2] and clearly exhibits classically impossible negative values around the center of the circularly symmetric (due to the undefined value of the phase) distribution. When the coherent seed is initially switched on at very low intensity ($|\alpha| \approx 0.4$, i.e., an average of one photon every seven pulses), the Wigner function starts to lose its circular symmetry while moving away from the origin due to the gradual appearance of a defined phase, but it still exhibits a clear nonclassical nature as indicated by its partial negativity (b). For increasing seed amplitudes, the negativity gradually gets less evident (c) and the ringlike wings in the distribution start to disappear making it more and more similar to the Gaussian typical of a classical coherent field (d). Interestingly, even at

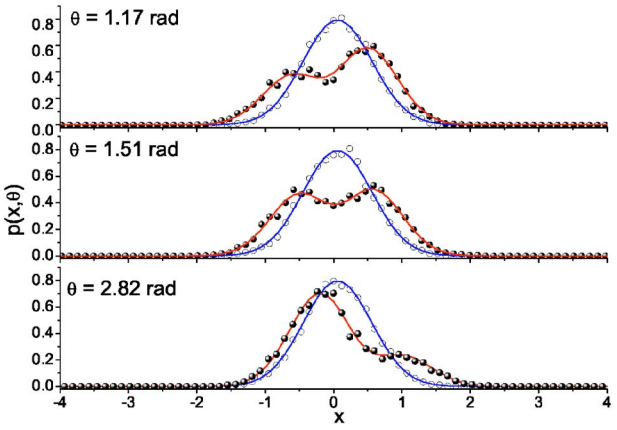


FIG. 6. (Color online) Normalized histograms of the pulse-integrated homodyne signal for the SPACS (filled circles) and the coherent seed field (empty circles) at different phases relative to the LO. The quadrature $x$ axis is normalized to the vacuum/coherent state distribution width. Also plotted (solid curves) are the fits to the theoretical curves for the Wigner marginals including the effects of the limited efficiency.

relatively high input amplitude $\alpha$, the Wigner distribution for the SPACS $|\alpha,1\rangle$ keeps showing the effect of the one-photon excitation when compared to the corresponding, slightly displaced, unexcited $|\alpha\rangle$ state [5].

When comparing the reconstructed Wigner functions and density matrix elements to the theoretical ones for the corresponding quantum states, one has to take into account the limited efficiency of the homodyne detection apparatus which does not allow one to generate and analyze pure states but always involves some mixing with the vacuum. The limited efficiency enters both in the preparation of the quantum state, where the dark counts and the nonideal conditioning in the idler channel do not allow one to generate a completely pure state in the signal channel, both in the homodyne detection process itself, due to the limited efficiency of the photodiodes and to the imperfect mode matching of the signal field with the LO [2].

Here the limited efficiency can be measured directly by studying the single-photon Fock state obtained by blocking the seed coherent field. The nonunit efficiency of the apparatus prevents the observation of the real single-photon Wigner function, and what one gets instead is its convolution with the vacuum one. The convolution result is the well-known $s$-parametrized quasiprobability distribution with the $s$ parameter scaled by the detection efficiency $\eta$ [22,24]. From a fit of the experimental quadrature distributions to the corresponding theoretical phase-independent, marginal curves, we obtain an overall efficiency of $\eta=0.602\pm0.002$.

The Wigner function of SPACSs in presence of limited efficiency is

$$W(z) = \frac{-2[2\eta - 1 - |2\sqrt{\eta}z - \alpha(2\eta - 1)|^2]}{\pi(1 + |\alpha|^2)} e^{-2|z - \sqrt{\eta}\alpha|^2} \tag{17}$$

and one can easily see that, as for single-photon Fock states, negative values can only be achieved with $\eta > 0.5$. The non-

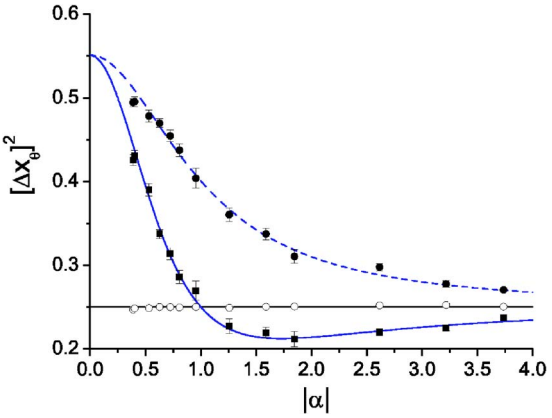


FIG. 7. (Color online) Variances of the squeezed (filled squares) and antisqueezed (filled circles) quadratures of the SPACS for different coherent state amplitudes. Solid and dashed lines are obtained from Eq. (20) with $\theta=0$ and $\theta=\pi/2$, respectively, and with a global efficiency set to $\eta=0.6$. Also shown are the experimental data (empty circles) and the theoretical curve (horizontal line at 1/4) for the variance of the coherent state.

unit detection efficiency thus reduces the nonclassical character of experimentally observed SPACSs and, especially for higher values of the seed amplitude $|\alpha|$, may completely mask it in the presence of reconstruction noise [see Fig. 5(d)]. In our case, a good efficiency combined with relatively low reconstruction errors allow us to clearly observe the nonclassical character of SPACSs up to $|\alpha|\approx 2$.

The marginal distributions of the SPACSs in the case of limited efficiency have the form

$$p(x,\theta,\alpha,\eta)=\frac{1}{1+|\alpha|^2}\sqrt{\frac{2}{\pi}}[1-\eta+4\eta x^2 + |\alpha|^2(1+2\eta(\eta-1)) - 4|\alpha|x\sqrt{\eta}(2\eta-1)\cos(\theta) + 2|\alpha|^2\eta(\eta-1)\cos(2\theta)]e^{-2(x-|\alpha|\sqrt{\eta}\cos\theta)^2} \tag{18}$$

and the corresponding mean values and variances have to be modified with respect to the ideal cases of Eqs. (7) and (8) as

$$\langle x_\theta\rangle_{\alpha,\eta}=\frac{|\alpha|(2+|\alpha|^2)\sqrt{\eta}\cos(\theta)}{1+|\alpha|^2} \tag{19}$$

and

$$[\Delta x_\theta]^2_{\alpha,\eta}=\frac{1}{4}+\frac{\eta[1-|\alpha|^2\cos(2\theta)]}{2(1+|\alpha|^2)^2}. \tag{20}$$

Figure 6 presents the experimental marginal distributions of the SPACS at a fixed value of the coherent seed amplitude $|\alpha|=0.387$ and for three different values of the phase $\theta$. Superposed to the data points are the curves obtained from a fit of the distributions to the expected shapes as given by Eq. (18).

The nonclassical character of SPACSs is also evident if the quadrature variances are measured for different amplitudes of the coherent seed field. Indeed, while the original coherent state has equal fluctuations in the different quadratures independently from its amplitude, the one-photon-excited state exhibits a squeezing in one of the quadratures and larger fluctuations in the orthogonal one as soon as $|\alpha|>1$, as indicated in Eqs. (8) and (20). An intuitive interpretation of this behavior can be connected with the reduction in the intensity noise of the coherent state when excited by a perfectly defined number of quanta with the corresponding increase in the phase noise due to the intrinsic lack of phase information of the Fock state. This effect starts to become evident in the reconstructed Wigner function of Fig. 5(c) (which is, however, still at the border of the unsqueezed region), where a somewhat reduced width appears along the radial direction, while the increase in the phase noise is indicated by the appearance of the ringlike wings in the tangential direction of the Wigner distribution. A more quantitative measurement of the variance in the squeezed and antisqueezed quadratures is presented in Fig. 7 where the expected curves for $\theta=0$ and $\theta=\pi/2$ are also drawn according to Eq. (20) with a global efficiency of $\eta=0.6$.

The experimental variances for the $x_{(\theta=0)}$ quadrature clearly get smaller than those of the corresponding coherent state (also shown in the graph and independent of the seed intensity) as soon as the amplitude exceeds unity, and a maximum squeezing of about 15% is obtained for $|\alpha|=1.85$.

The density matrix elements reconstructed from the data can also be compared with the theoretical ones provided that a Bernoulli transformation

$$\rho'_{i,j}=\eta^{(i+j)/2}\sum_{k=0}^{\infty}\left[\binom{i+k}{i}\binom{j+k}{j}\right]^{1/2}(1-\eta)^k\rho_{i,j} \tag{21}$$

is performed in order to include the effects of non-unit efficiency. The expected density matrix $\rho_c$ is thus obtained from Eqs. (4) and (21) with $\eta=0.6$. Figure 8 shows the calculated density matrix elements and the corresponding Wigner func-

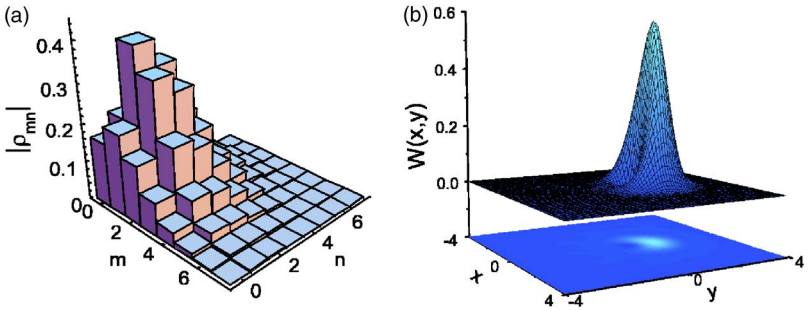


FIG. 8. (Color online) (a) Calculated density matrix elements and (b) Wigner function of the SPACS in the case of limited efficiency ($\eta=0.6$) and for $|\alpha|=0.955$.

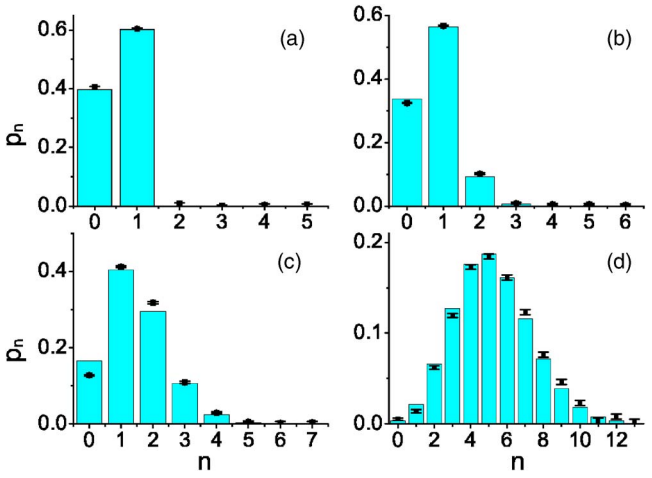


FIG. 9. (Color online) Experimental (data points with error bars) and theoretical (solid bars) photon number distributions for the SPACS in the case of limited efficiency ($\eta$=0.6). (a) $|\alpha|$=0, (b) $|\alpha|$=0.387, (c) $|\alpha|$=0.955, (d) $|\alpha|$=2.61.

tion for the SPACS with $|\alpha|$=0.955. Such data should be compared to the experimental plots of Figs. 4(c) and 5(c). The theoretical and experimental photon number distributions for the SPACS with increasing seed amplitudes $|\alpha|$ are also plotted in Fig. 9 where the errors have been calculated as in Ref. [23].

In order to better quantify the agreement of the experimental results with the theoretical ones, we calculated the purity $P$ of the reconstructed states and compared it with the expected one $P_c$. The purity tends to increase with the amplitude of the seed coherent field as the final state evolves from a mixture of vacuum and single photon towards a pure coherent one. Results are presented in Table I, where we also show the fidelity of the reconstructed states to the theoretical ones, calculated as proposed by Jozsa [25] for the comparison between mixed quantum states

$$F \equiv |\mathrm{Tr}[\sqrt{\sqrt{\rho_c}\rho_e\sqrt{\rho_c}}]|^2, \tag{22}$$

where $\rho_e$ is the experimentally derived density matrix.

A comparison of the fidelity values with the photon number distributions of Fig. 9 seems to indicate that fidelity, quickly saturating to unity even for somewhat different distributions, is not a very sensitive benchmark for the closeness of the experimental to the expected states in this case. A similar conclusion has been recently obtained by the group of Kwiat [26] in the case of depolarized entangled mixed states in the discrete variable domain.

## VII. CONCLUSIONS

We have successfully used a conditional preparation technique to generate a new class of light states whose degree of nonclassicality can be continuously tuned between the extreme situations of pure quantum states and classical ones. Such single-photon-added coherent states are particularly interesting from a fundamental point of view as they represent the result of the most elementary excitation of a classical light field. In this regard, the demonstrated possibility to follow their evolution so closely will certainly push the experimental research towards the investigation of other interesting and equally fundamental quantum processes. Single-photon-added coherent states are also noteworthy because, for the first time to our knowledge, both the typical properties of a quantum character, i.e., the negativity of the Wigner function combined with a quadrature squeezing, are simultaneously and clearly observed in a light state. While the nonclassicality criterion based on the squeezing can be in principle fulfilled without bounds on the detection efficiency, as shown in Eq. (20), the negativity of the Wigner function is a much stricter criterion since it requires efficiencies higher than 50%. We have demonstrated the possibility of using our recently developed technique for high-frequency time-resolved balanced homodyne detection to reconstruct the density matrix elements and the Wigner functions of the generated states with an overall efficiency of 60%. Thanks to the very high acquisition rates achievable by our system, other nonclassical states, particularly those involving higher number of photons and normally characterized by lower generation efficiencies, are within reach for a complete tomographic analysis.

TABLE I. Quantum state indicators for SPACSs. $M$ dimension of the reconstructed density matrix; $P_c$ expected purity for the state; $P$ purity of the reconstructed state; $F$ fidelity between the experimentally reconstructed and the expected state.

| $\|\alpha\|$ | $M$ | $P_c \equiv \mathrm{Tr}(\rho_c^2)$ | $P \equiv \mathrm{Tr}(\rho_c^2)$ | $F$ |
|---|---|---|---|---|
| 0 | 6 | 0.52 | 0.53±0.01 | 1.009±0.004 |
| 0.387 | 7 | 0.64 | 0.63±0.01 | 0.990±0.004 |
| 0.955 | 8 | 0.87 | 0.83±0.02 | 0.976±0.004 |
| 2.61 | 14 | 0.99 | 1.02±0.05 | 0.995±0.005 |

## ACKNOWLEDGMENTS

This work has been performed in the frame of the "Spettroscopia laser e ottica quantistica" project of the Department of Physics of the University of Florence and partially supported by the Italian Ministry of University and Scientific Research (MIUR), under the FIRB Contract No. RBNE01KZ94.

[1] A. I. Lvovsky, H. Hansen, T. Aichele, O. Benson, J. Mlynek, and S. Schiller, Phys. Rev. Lett. **87**, 050402 (2001).
[2] A. Zavatta, S. Viciani, and M. Bellini, Phys. Rev. A **70**, 053821 (2004).
[3] A. I. Lvovsky and S. A. Babichev, Phys. Rev. A **66**, 011801(R) (2002).
[4] J. Wenger, R. Tualle-Brouri, and P. Grangier, Phys. Rev. Lett. **92**, 153601 (2004).
[5] A. Zavatta, S. Viciani, and M. Bellini, Science **306**, 660 (2004).
[6] A. P. Lund, H. Jeong, T. C. Ralph, and M. S. Kim, Phys. Rev. A **70**, 020101(R) (2004).
[7] M. Dakna, L. Knöll, and D.-G. Welsch, Eur. Phys. J. D **3**, 295 (1998).
[8] G. S. Agarwal and K. Tara, Phys. Rev. A **43**, 492 (1991).
[9] D. N. Klyshko, Sov. J. Quantum Electron. **7**, 591 (1977).
[10] G. K. Kitaeva, A. N. Penin, V. V. Fadeev, and Y. A. Yanait, Sov. Phys. Dokl. **24**, 564 (1979).
[11] A. Migdall, Phys. Today **52**, 41 (1999).
[12] K. J. Resch, J. S. Lundeen, and A. M. Steinberg, Phys. Rev. Lett. **88**, 113601 (2002).
[13] Z. Y. Ou, L. J. Wang, and L. Mandel, J. Opt. Soc. Am. B **7**, 211 (1990).
[14] F. De Martini, V. Mussi, and F. Bovino, Opt. Commun. **179**, 581 (2000).
[15] Z. Y. Ou, Quantum Semiclassic. Opt. **9**, 599 (1997).
[16] T. Aichele, A. I. Lvovsky, and S. Schiller, Eur. Phys. J. D **18**, 237 (2002).
[17] M. Bellini, F. Marin, S. Viciani, A. Zavatta, and F. T. Arecchi, Phys. Rev. Lett. **90**, 043602 (2003).
[18] S. Viciani, A. Zavatta, and M. Bellini, Phys. Rev. A **69**, 053801 (2004).
[19] S. Reynaud, A. Heidmann, E. Giacobino, and C. Fabre, in *Progress in Optics*, edited by E. Wolf (Elsevier, Amsterdam, 1992), Vol. 30, p. 1.
[20] A. Zavatta, M. Bellini, P. L. Ramazza, F. Marin, and F. T. Arecchi, J. Opt. Soc. Am. B **19**, 1189 (2002).
[21] K. Vogel and H. Risken, Phys. Rev. A **40**, R2847 (1989).
[22] U. Leonhardt, *Measuring the Quantum State of Light* (Cambridge University Press, Cambridge, England, 1997).
[23] G. M. D'Ariano, in *Quantum Optics and Spectroscopy of Solids*, edited by T. Hakioğlu and A. S. Shumovsky (Kluwer Academic Publishers, Dordrecht, 1997), pp. 175–202.
[24] L. Mandel and E. Wolf, *Optical Coherence and Quantum Optics* (Cambridge University Press, Cambridge, England, 1995).
[25] R. Jozsa, J. Mod. Opt. **41**, 2315 (1994).
[26] N. A. Peters, T. C. Wei, and P. G. Kwiat, Phys. Rev. A **70**, 052309 (2004).